Electronic Supplementary Material (ESI) for Physical Chemistry Chemical Physics.


# Deciphering binding mechanism of inhibitors to SARS-COV-2 main protease through multiple replica accelerated molecular dynamics simulations and free energy landscapes

Meng Li,[a] Xinguo Liu,*[a] Shaolong Zhang,[a] Shanshan Liang,[a] Qinggang Zhang[a] and Jianzhong Chen*[b,c]

* [a]School of Physics and Electronics, Shandong Normal University, Jinan, China, 250358, E-mail: liuxinguo@sdnu.edu.cn.
[b]School of Science, Shandong Jiaotong University, Jinan, China, 250357, E-mail: jzchen@sdjtu.edu.cn, chenjianzhong1970@163.com
[c]Shandong Key Laboratory of Biophysics, Institute of Biophysics, Dezhou University, Dezhou 253023, China

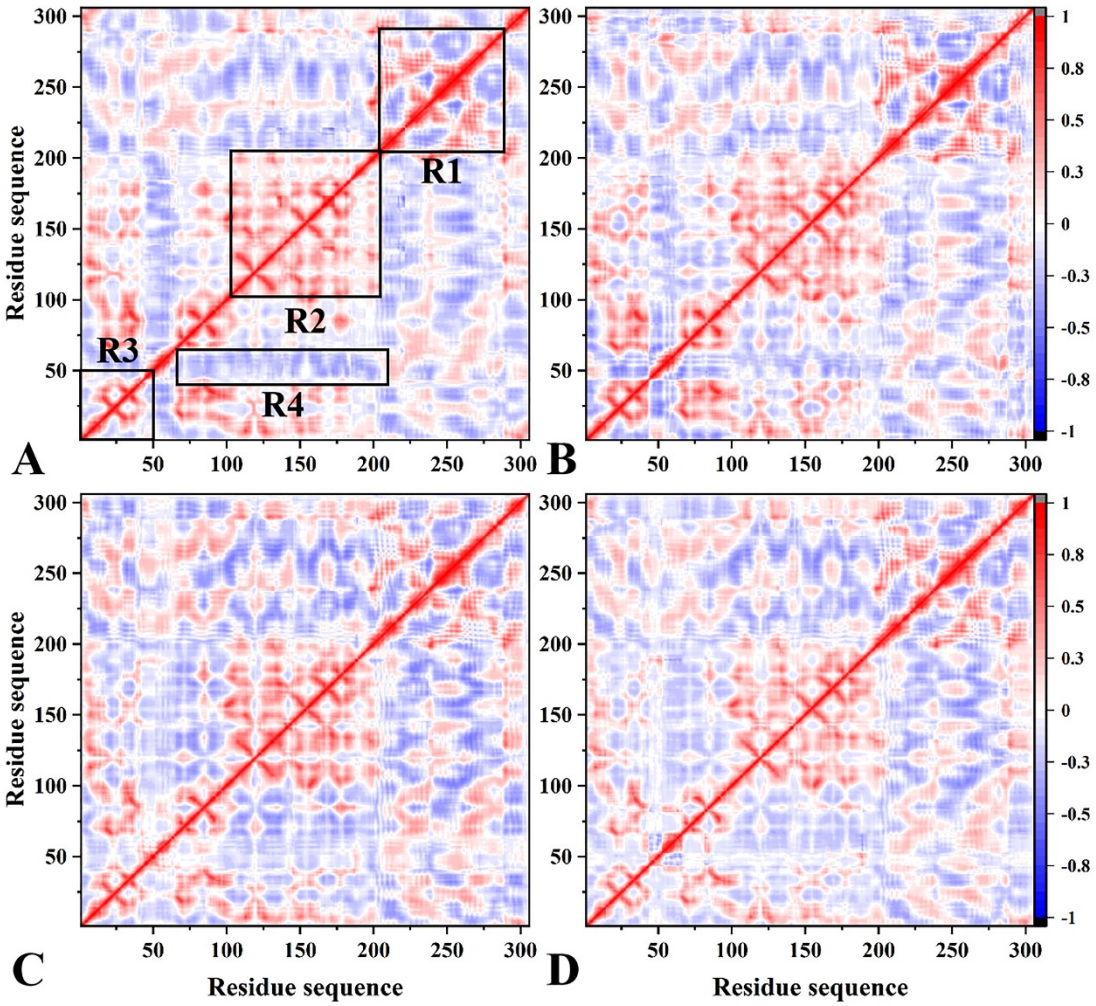


**Fig. S1** Dynamic cross-correlation maps calculated by using the coordinates of the $C_\alpha$ atoms from MR-aMD trajectories in the monomer B: (A), (B), (C) and (D) respectively corresponding to the *apo*, YTV-, YSP- and YU4-bound $M^{pro}$. Inhibitor binding affects the motion pattern of the Mpro, and black boxes indicate areas where the motion pattern is highly variable.

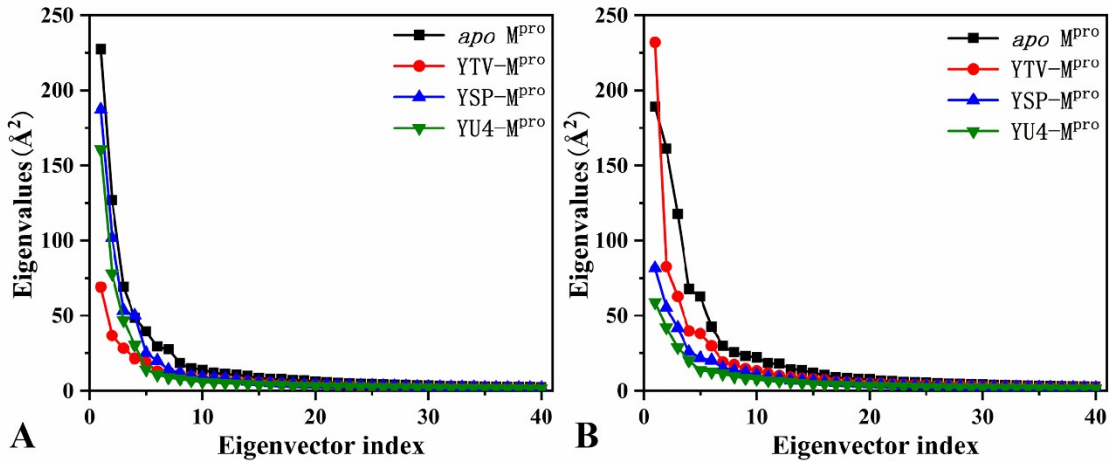


**Fig. S2** The function of the eigenvalues VS the eigenvector indices obtained from principal component analysis performed on the single connected MR-aMD trajectory: (A) and (B) respectively corresponding to the $M^{pro}$ monomer A and the $M^{pro}$ monomer B. In general, the combination of YTV, YSP and YU4 weakened the movement of $M^{pro}$.

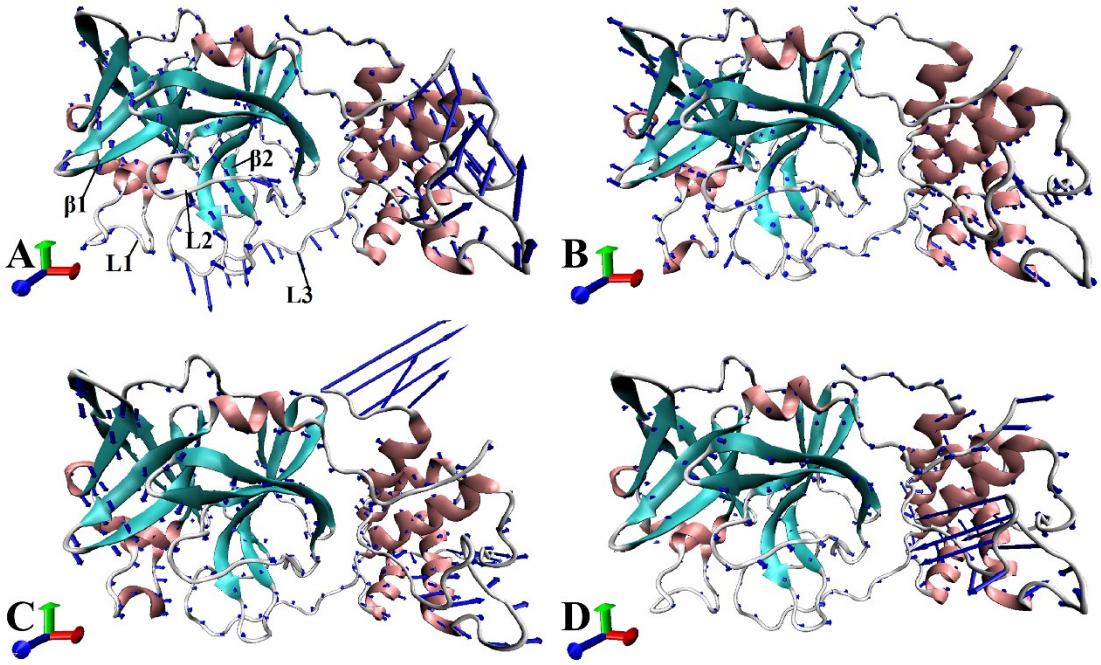


**Fig. S3** Collective motions of domains in the $M^{pro}$ monomer B along the first eigenvector resulting from basic dynamics analysis: (A) the *apo* state of $M^{pro}$, (B) the YTV-bound $M^{pro}$, (C) the YSP-bound $M^{pro}$, and (D) the YU4-bound $M^{pro}$. The direction and length of the arrows in this diagram reflect the motion direction and strength of domains in the $M^{pro}$, respectively. The binding of YTV, YSP and YU4 has a significant effect on the movement of β-sheet β1, β2 and loops L1, L2 and L3 in $M^{pro}$.

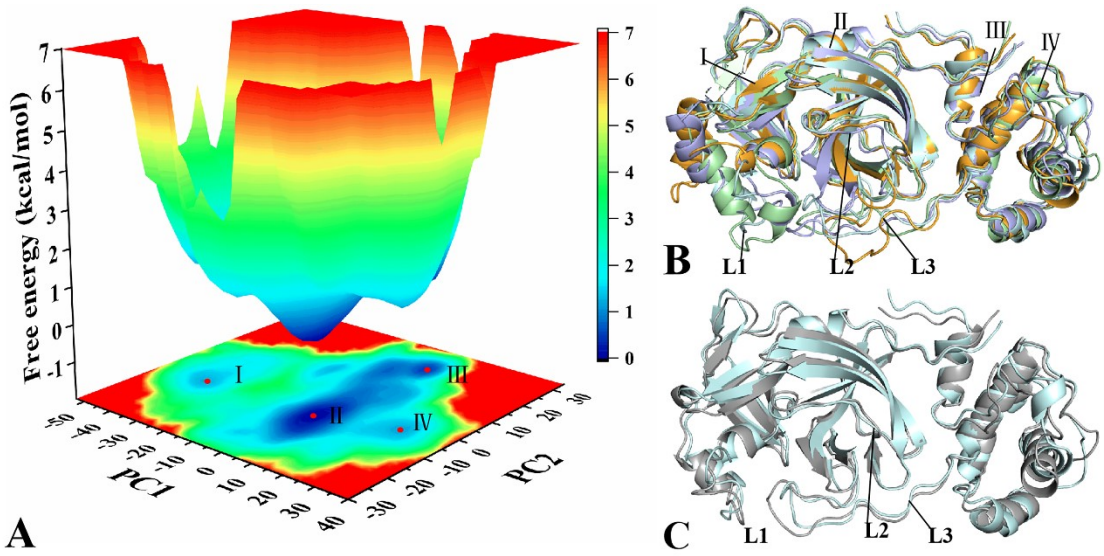


**Fig. S4** Free energy landscape and representative structures of the *apo* state of the M$^{pro}$ monomer B: (A) the free energy landscape of the *apo* M$^{pro}$, (B) the superposition of the four representative structures corresponding to the four energy basins I, II, III and IV, (C) the superposition of the representative structure at the lowest energy basin with the crystal structure.

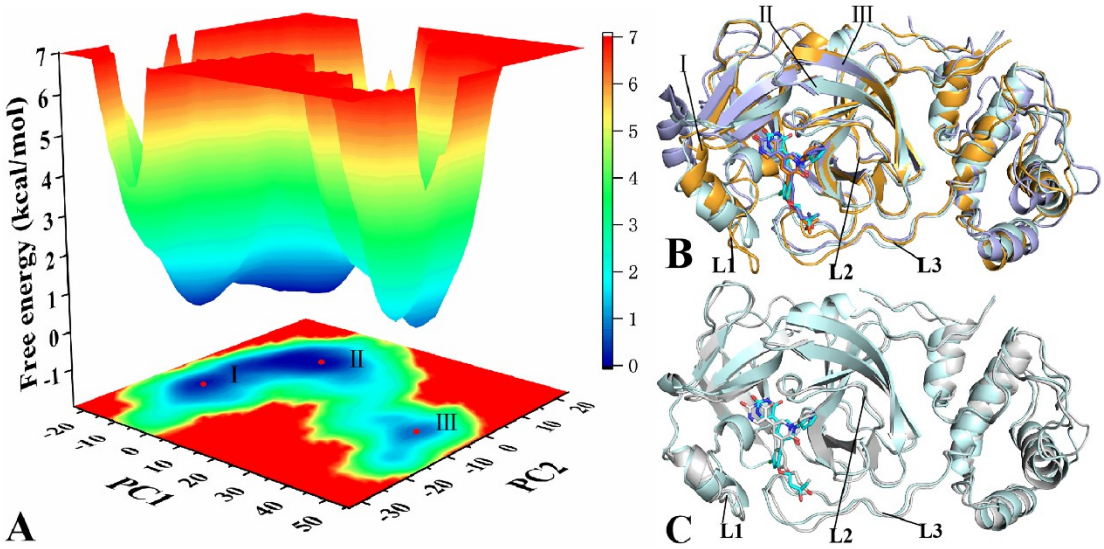


**Fig. S5** Free energy landscape and representative structures of the YTV-bound M$^{pro}$ monomer B: (A) the free energy map of the YTV-bound M$^{pro}$, (B) the superposition of the three representative structures located at the three energy basins I, II and III and (C) the superimposition of the representative structure and the crystal structure.

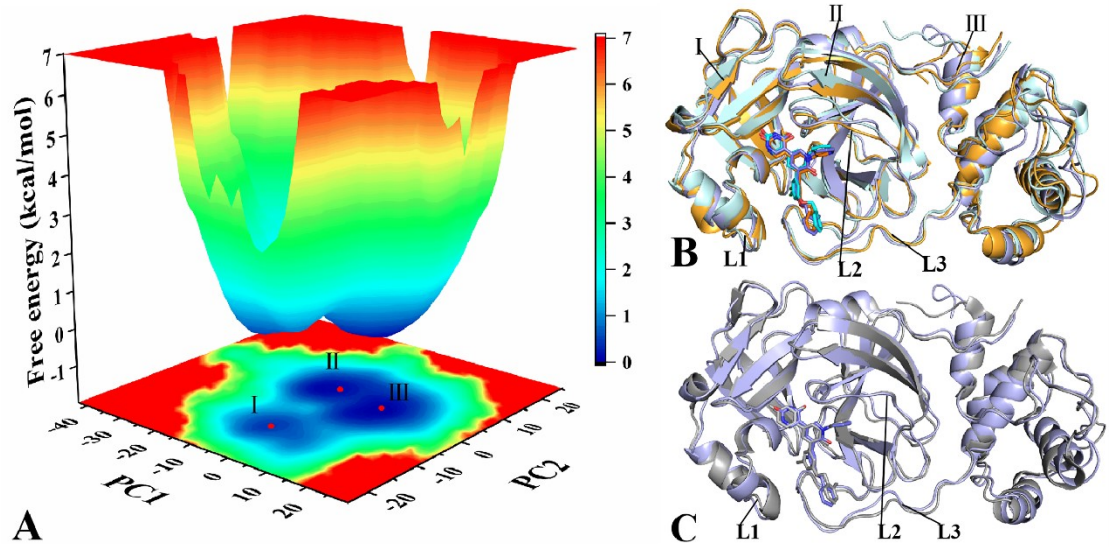


**Fig. S6** Free energy landscape and the representative structure of YSP-bound M$^{pro}$ monomer B: (A) the free energy landscape of the YSP-bound M$^{pro}$, (B) the superposition of the three representative structures situated at the three energy basins I, II and III, (C) the superposition of the representative structures at the lowest energy basin with the crystal structure.

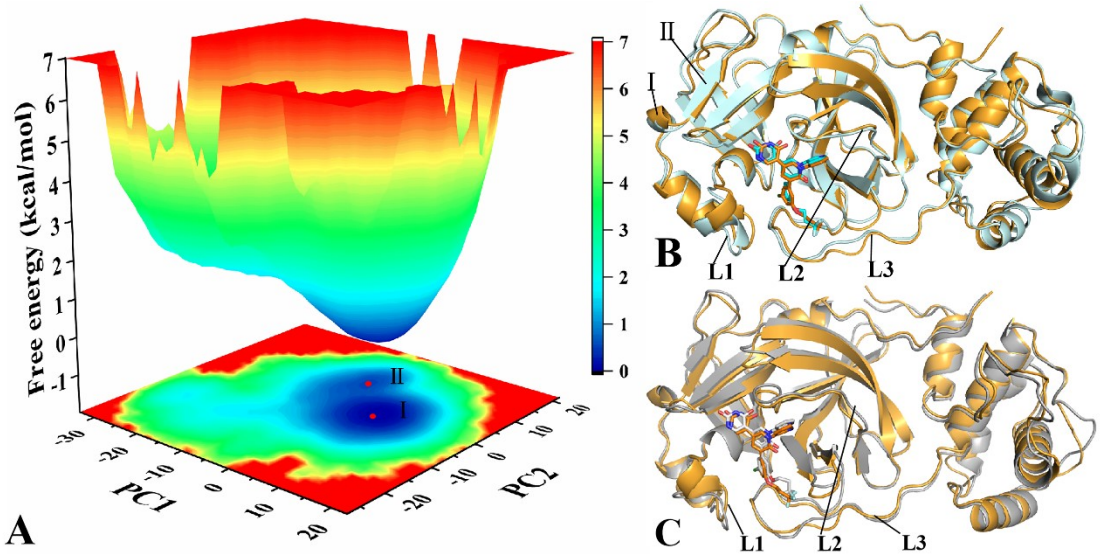


**Fig. S7** Free energy landscape and representative structures of the YU4-bound $M^{pro}$ monomer B: (A) the free energy landscape of the YU4-bound $M^{pro}$, (B) the representative structure of energy basin I, (C) the superposition of the representative structure at the lowest energy basin with the crystal structure.

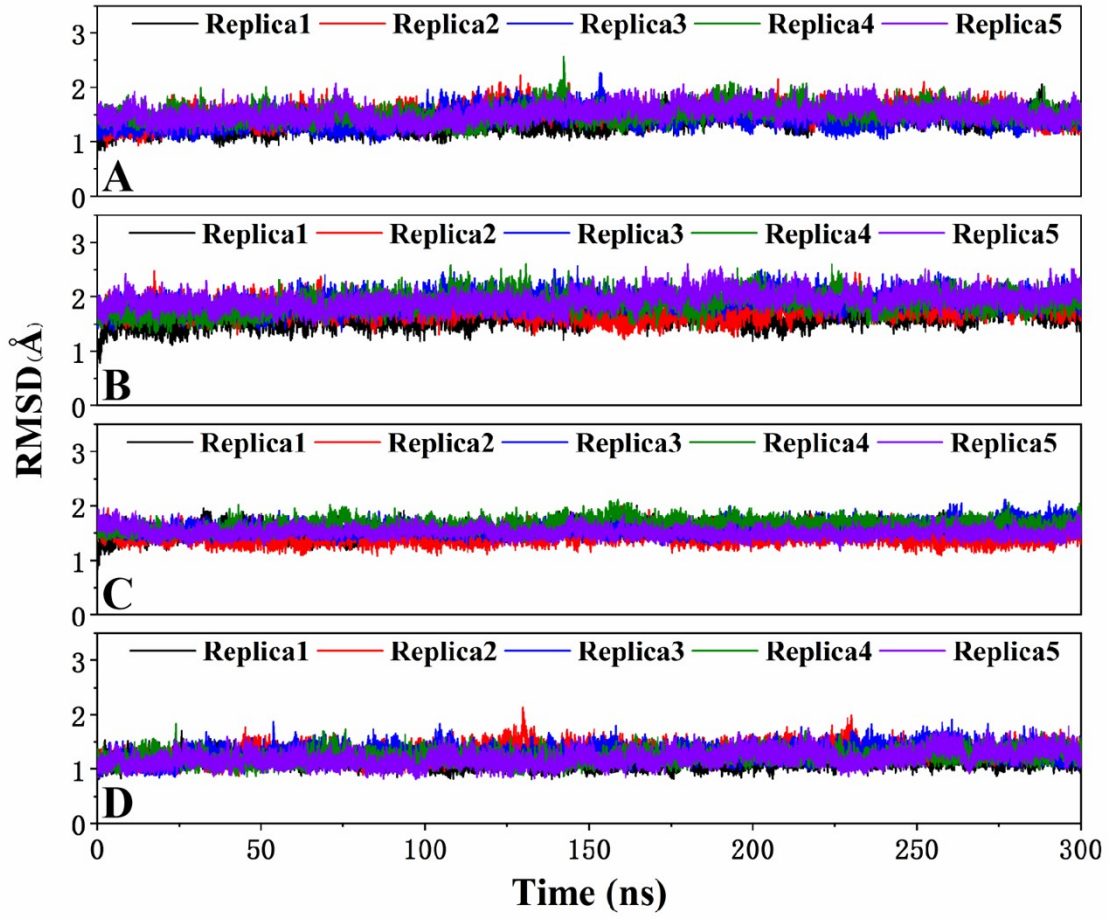


**Fig. S8** Root-mean-square deviations (RMSDs) of backbone atoms in the $M^{pro}$: (A) the *apo* $M^{pro}$, (B) the YTV-bound $M^{pro}$, (C) the YSP-bound $M^{pro}$ and (D) the YU4-bound $M^{pro}$. Five replicas of the cMD simulation for the last 200ns reached equilibrium.

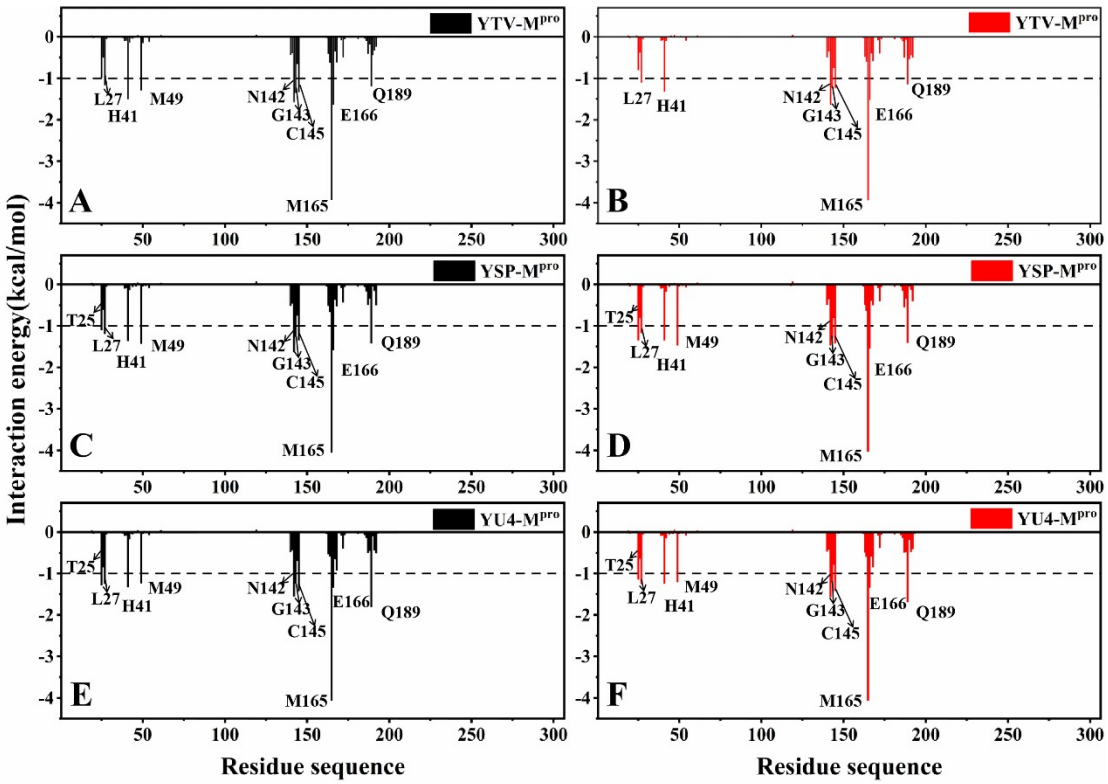


**Fig. S9** Interactions of inhibitors with separate residues in the $M^{pro}$: (A), (C) and (E) respectively corresponding to the $M^{pro}$ monomer A complexed with YTV, YSP and YU4, (B), (D) and (F) respectively relating with the $M^{pro}$ monomer B complexed with YTV, YSP and YU4. Significant residues with an energy contribution greater than 1.0 kcal/mol were flagged.

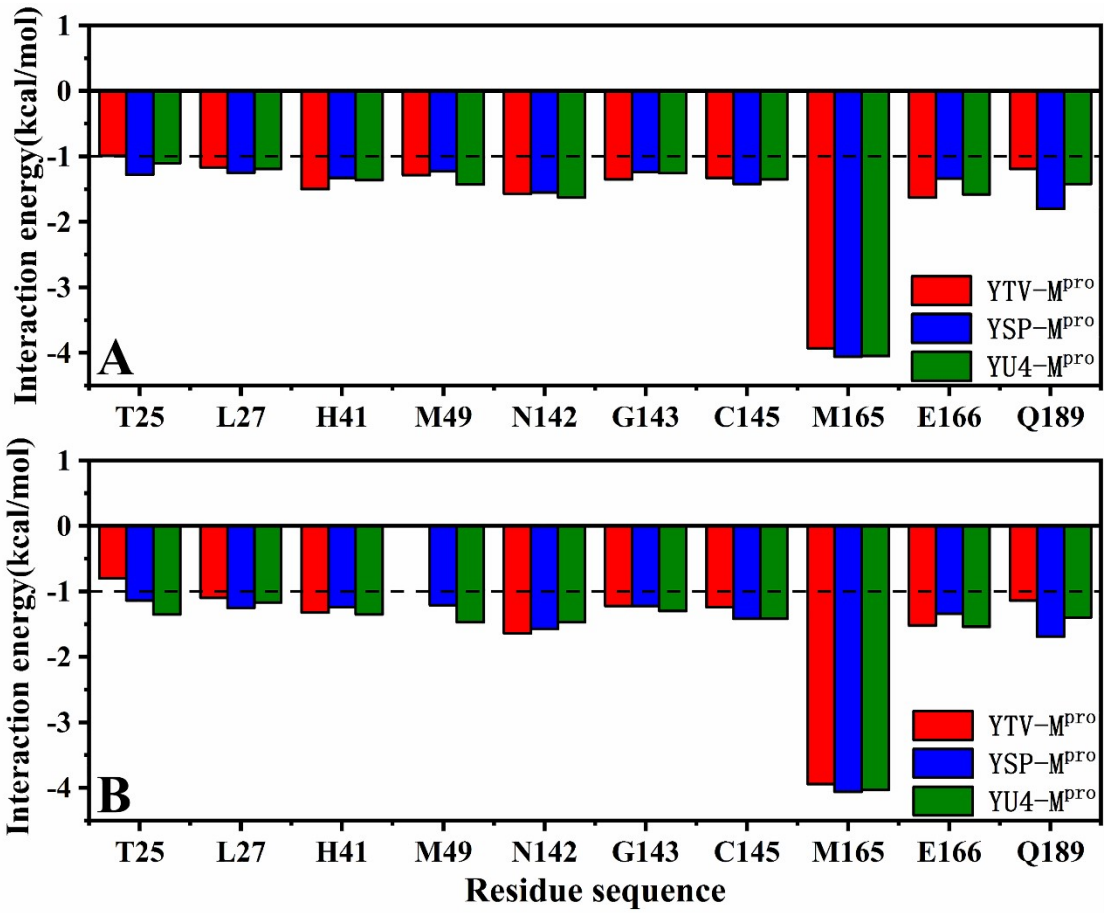


**Fig. S10** Interactions of inhibitors with significant residues in the $M^{pro}$: (A) and (B) respectively corresponding to the $M^{pro}$ monomer A and the $M^{pro}$ monomer B.

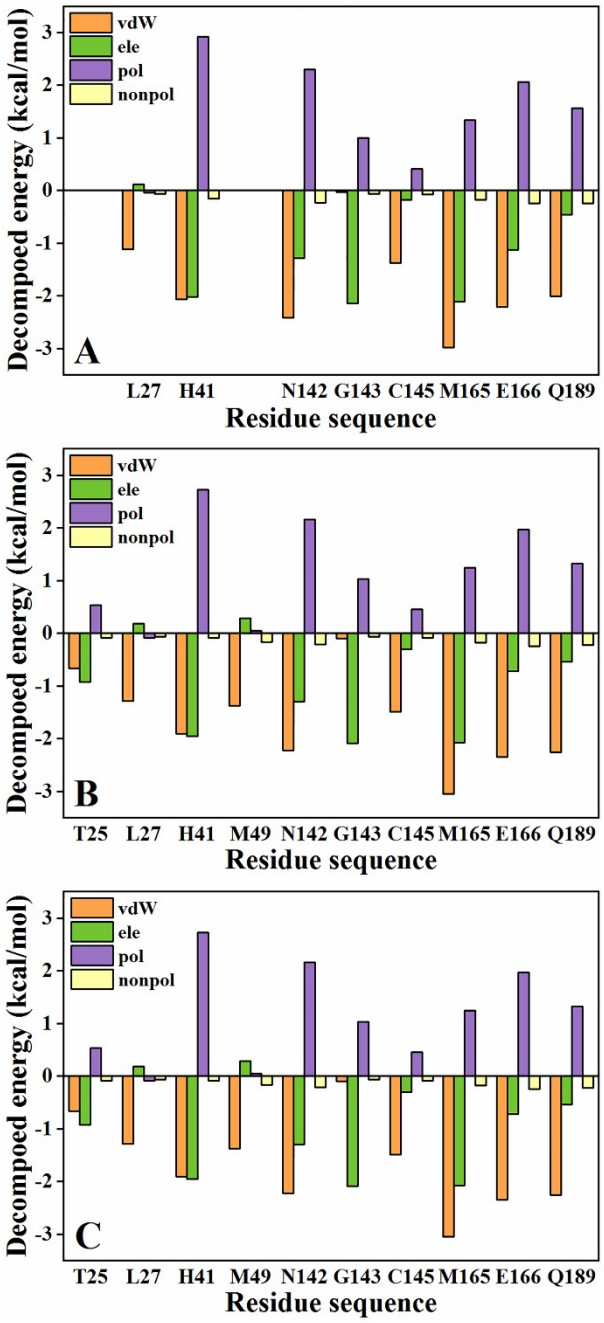


**Fig. S11** Interaction energies of inhibitors with key residues in the $M^{pro}$ monomer B was decomposed into electrostatic energy, van der Waals energy, polar solvation energy and nonpolar solvation energy: (A) the YTV-bound $M^{pro}$, (B) the YSP-bound $M^{pro}$ and (C) the YU4-bound $M^{pro}$. The favorable energy contributions between residues and inhibitors derived originate from van der Waals and electrostatic energy.

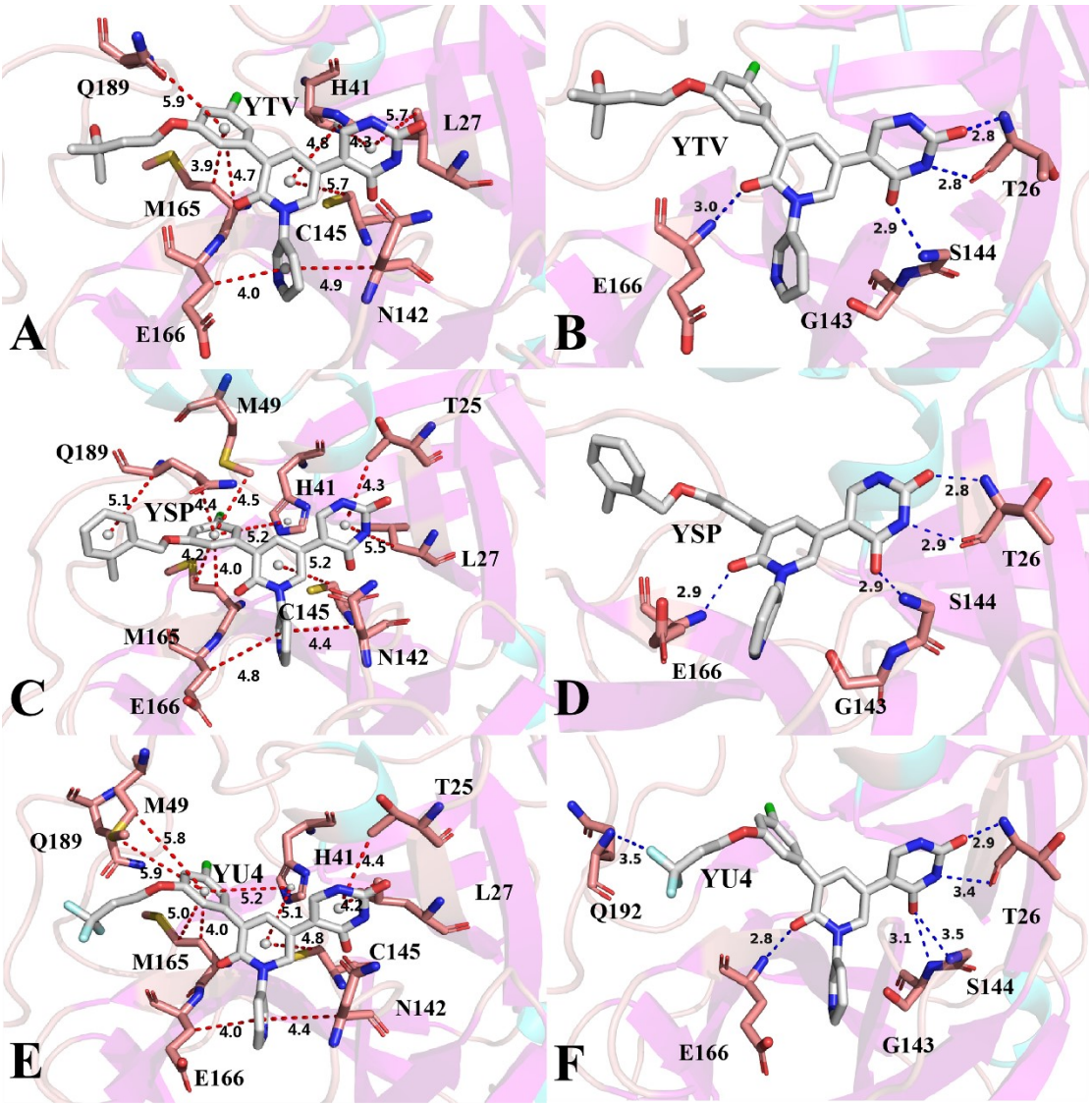


**Fig. S12** Geometric positions of inhibitors relative to key residues in the M$^{pro}$ monomer B: (A) and (B) separately corresponding to hydrophobic interactions and hydrogen bonding interactions of YTV with the M$^{pro}$, (C) and (D) respectively displaying hydrophobic interactions and hydrogen bonding interactions of YSP with the M$^{pro}$, and (E) and (F) separately indicating hydrophobic interactions and hydrogen bonding interactions of YU4 with the M$^{pro}$.